AIAA JOURNAL
Vol. 44, No. 7, July 2006

Aerodynamic Force Generation in Hovering Flight in a Tiny Insect

Mao Sun* and Xin Yu†
Beijing University of Aeronautics and Astronautics, Beijing 100083, People's Republic of China

Aerodynamic force generation in hovering flight in a tiny insect, *Encarsia formosa*, has been studied. The Reynolds number of the flapping wings (based on the mean chord length and the mean flapping velocity) is around 15. The flapping motion of the insect is unique in that the wing pair "claps" together near the end of an upstroke and "flings" open at the beginning of the subsequent downstroke. The method of solving the Navier–Stokes equations over moving overset grids is used. The fling produces a large lift peak at the beginning of the downstroke, the mechanism of which is the generation of a vortex ring containing a downward jet in a short period; the clap produces a large lift peak near the end of the subsequent upstroke by a similar mechanism. Because the vorticity generated during the clap and fling diffuses rapidly, the clap and fling has little influence on the flows in the rest part of the stroke cycle. The mean lift is enough to support the weight of the insect. The lift peaks due to the clap and fling result in more than 30% increase in mean lift coefficient compared to the case of flapping without clap and fling.

Nomenclature

C_D	=	drag coefficient
$\bar{C}_D$	=	mean drag coefficient
C_L	=	lift coefficient
$\bar{C}_L$	=	mean lift coefficient
c	=	mean chord length of wing
D	=	drag of a wing
d	=	distance between the two wings at start of a stroke
G	=	weight of the insect
L	=	lift of a wing
n	=	wingbeat frequency
p	=	nondimensional fluid pressure
R	=	wing length
Re	=	Reynolds number, cU/ν
r_2	=	radius of the second moment of wing area
S	=	area of one wing
t	=	time
U	=	reference velocity (mean flapping velocity)
u, v, w	=	x, y, z components of nondimensional flow velocity, respectively
W	=	velocity of upward motion of wings near the end of a stroke
x, y, z	=	coordinates in inertial frame of reference
x', y', z'	=	coordinates in noninertial frame of reference
α	=	geometric angle of attack
α_m	=	midstroke geometric angle of attack
$\dot{\alpha}$	=	angular velocity of flip
$\dot{\alpha}^+$	=	nondimensional angular velocity of flip
$\Delta\tau_r$	=	duration of wing rotation or flip duration (nondimensional)
$\dot{\theta}_c$	=	angular velocity of clap
$\dot{\theta}_f$	=	angular velocity of fling
ν	=	kinematic viscosity
ξ, η, ζ	=	computational coordinates
ρ	=	density of fluid
τ	=	nondimensional time
$\hat{\tau}$	=	nondimensional time during one stroke cycle
Φ	=	stroke amplitude
$\dot{\phi}$	=	angular velocity of azimuthal rotation
$\dot{\phi}^+$	=	nondimensional angular velocity of azimuthal rotation

Received 26 April 2005; revision received 6 December 2005; accepted for publication 12 December 2005.

*Professor, Institute of Fluid Mechanics; m.sun@263.net.
†Graduate Student, Institute of Fluid Mechanics.

I. Introduction

IT has been shown that classical steady-state aerodynamic theories could not explain the generation of large lift by the wing of small insects and that unsteady aerodynamic mechanisms must be employed. (For reviews, see Refs. 1–3.) One of the unsteady mechanisms is known as the "clap and fling" mechanism, proposed by Weis-Fogh[4] based on observation of the small wasp *Encarsia formosa* hovering. Some other small insects, for example, fruitfly *Drosophila virilis*, have also been observed employing the clap and fling mechanism in some circumstances.[5,6]

The wingbeat cycle of the *Encarsia formosa* is summarized as follows. Before the start of a wingbeat cycle, the two wings are close together (Fig. 1a). The wingbeat cycle begins with the fling phase, during which the wings open to form a V shape by rotating about their trailing edges (Fig. 1b). Following the fling, the two wings separate and move in opposite directions around the body (termed downstroke translation; Fig. 1c). After moving apart through a certain distance, the wings flip around so that the undersides of the wings become their top sides and vice versa (Fig. 1d). Following the flip phase, the wings move dorsally toward each other (termed upstroke translation; Fig. 1e). When their leading edges are near each other, the wings clap, that is, rotate about their leading edges (Fig. 1f) so that their trailing edges are brought together and then the wings return to their initial position. Normal hovering insects beat their wings back and forth in a horizontal plane, and the movement of the wings is similar to that just described except that there is no clap and fling motion, that is, the dorsal flip is similar to the ventral flip. Weis-Fogh[4] found that the high lift required in the hovering in *Encarsia formosa* could not be explained on the basis of conventional aerodynamic theories. He suggested that the fling of each wing generates a circulation around it. Because of the symmetry of the motion, the magnitudes of the two circulations about the two wings are equal and the senses are opposite. One wing with its circulation acts like the starting vortex of the other wing and vice versa, then no starting vortices need to be shed as the wings move apart. Weis-Fogh argued that this absence of starting vortices avoids the delay in the buildup of the maximum lift force required by the Wagner effect and brings about a high overall lift over the wingbeat cycle. Lighthill[7] modeled the fling phase

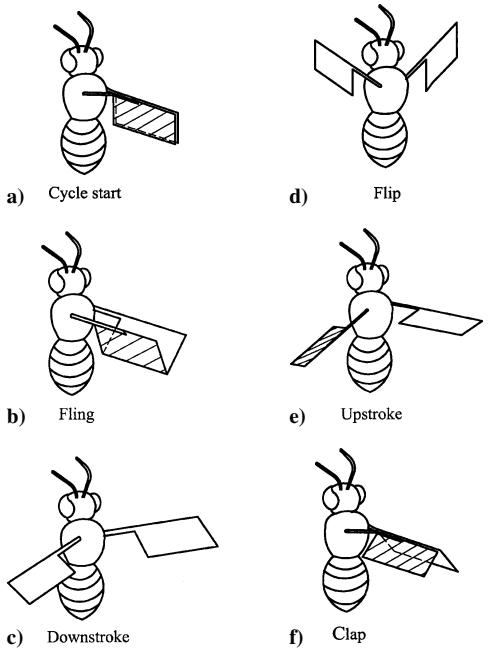

Fig. 1 Flapping motion of *Encarsia formosa*.

using two-dimensional inviscid theory. He obtained a circulation around the airfoil that is proportional to the angular velocity of the airfoils, without the delay associated with the Wagner effect. Lighthill's analysis provides theoretical basis for the Weis-Fogh mechanism.

Maxworthy,[8] by a flow visualization experiment on a pair of wings, discovered that during the fling phase a leading-edge vortex (LEV) is generated on each wing and the magnitude of its circulation is substantially larger than that calculated by Lighthill's inviscid theory. In view of Maxworthy's results, Edwards and Cheng[9] improved Lighthill's theory of the fling motion by adding a pair of point vortices to the invicid model to represent the LEVs. The strength of the vortices is determined in the solution process. The calculated vortex strength agrees with Maxworthy's experiment results. Wu and Chen[10] also formulated a model of invicid flow plus a pair of vortices. The calculated vortex strength from their model is very close to that of Edwards and Cheng,[9] and lift and drag forces on the airfoils are also provided. Spedding and Maxworthy[11] measured the unsteady lift on a pair of airfoils performing the fling motion and showed that the lift coefficient increased from 0 to about 5 as the opening angle increases from 0 to π. Simultaneous flow visualization was used to measure the circulation of the LEV. Their results show that the large lift coefficient is associated with the high circulation around the LEV. The measured lift coefficient is in good agreement with that calculated by Wu and Chen.[10]

Recently aerodynamic force in the fling and the subsequent translation phases have been studied by Ro and Tsutahara[12] for a wing pair using a discrete vortex method and by Sun and Yu[13] and Miller and Peskin[14] for an airfoil pair using computational fluid dynamics (CFD). Very large lift is produced during the fling phase. Lift coefficient in the translation phase is much smaller; nevertheless, it is large compared to the steady-state values.

In the cited works, either the fling or the fling and the subsequent translation were studied. To our knowledge, the complete cyclic flapping motion of the wing pair in the tiny insect *Encarsia formosa* has not been investigated. There still exist questions such as how the aerodynamic force on the wings varies with time in a complete cycle and whether the mean lift is large enough for weight support. In the present study, the aerodynamic forces and the flow around a model wing pair performing the complete cyclic flapping motion of *Encarsia formosa* is investigated by solving the Navier–Stokes equations numerically. Because of the unique feature of the motion, that is, the two wings are close together at the beginning of each flapping cycle and then move apart through a large distance, the approach of solving the flow equations over moving overset grids is chosen.

II. Methods

A. Model Wings and Their Motion

The model wings used in the present study are flat plates with rounded leading and trailing edges. The thickness of the plate is 1% of c, where c is the mean chord length, and the leading or trailing edge radius is 0.5% of c. The planform of the model wings (Fig. 2a) is similar to that of an entire wing of *Encarsia Formosa*, which consists of the membrane and the brim of marginal hairs.[15] On the basis of the estimate of the thickness of the boundary layer around the brim hairs, Ellington[15] pointed out that the hairs might extend the wing area close to their distal ends. Recently, Sunada et al.[16] did experiment on a bristled wing and a solid wing of the same planform performing starting motion from rest, $Re = 12$. They found that the aerodynamic forces on the bristled wing were approximately the same as those of the solid wing, showing that, at such low Reynolds number Re, the hairs could act as membrane.

The motion of the wings is shown in Figs. 2b–2d. Because the motion of the wing pair is symmetrical about the middle plane, we only describe the motion of the right wing. Two coordinate systems are used (Fig. 2). One is the inertial system, $oxyz$. The origin coincides with the base of the right wing at the start of a cycle, the oxy plane is horizontal (parallel to the stroke plane), the y axis points to the right of the insect, the x axis points backward, and the z axis is vertical. The other is the body-fixed coordinate system, $o'x'y'z'$, which rotates with the wing. The x' axis is parallel to the wing chord, and the y' axis is on the flip axis of the wing. At the start of a cycle, the two wings are close to each other, with their chord lines in a vertical direction. On the basis of data given by Weis-Fogh[4] and Ellington,[15] the flapping motion is approximated as follows. At the beginning of a cycle, the wing rotates about its trailing edge with angular velocity $\dot{\theta}_f$ (the fling); near the end of the fling phase, the wing begins to rotate around a vertical axis passing the wing root with angular velocity $\dot{\phi}$ (downstroke); at the end of the downstroke, the wing flips, that is, rotates around the flip axis with angular velocity $\dot{\alpha}$; after the flip, the wing rotates around the vertical axis (upstroke); near the end of the upstroke (with the leading edges of the two wings now close to each other), the wing rotate about its leading edge with angular velocity $\dot{\theta}_c$ (the clap); near the end of the clap (with the two wings now almost in vertical planes and close to each other), the

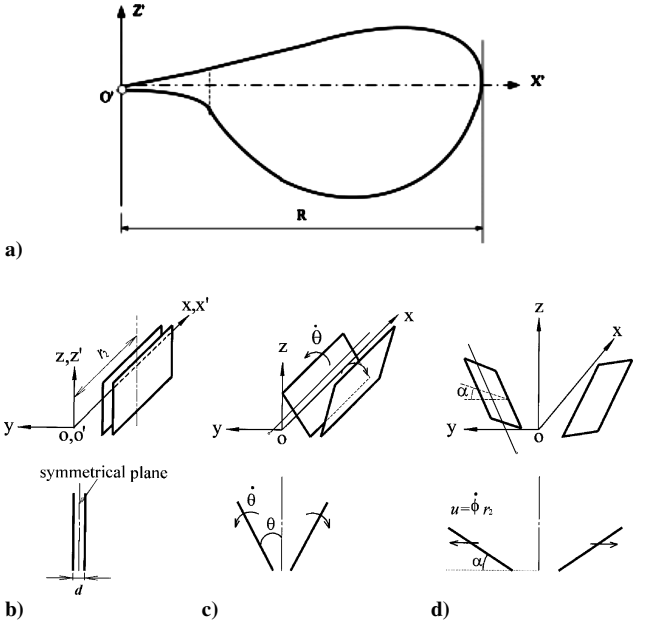

Fig. 2 Motion and reference frames.

wing pair moves vertically up for a small distance to return to its beginning position of the cycle. The angular velocities of the fling, the flip, and the clap are given as, respectively,

$$\dot{\theta}_f^+ = \dot{\theta}_f c/U = 0.5\dot{\theta}_0^+\{1 - \cos[2\pi(\tau - \tau_0)/\Delta\tau_f]\}$$
$$\tau_0 \le \tau \le \tau_0 + \Delta\tau_f \quad (1)$$

$$\dot{\alpha}^+ = \dot{\alpha} c/U = 0.5\dot{\alpha}_0^+\{1 - \cos[2\pi(\tau - \tau_r)/\Delta\tau_r]\}$$
$$\tau_r \le \tau \le \tau_r + \Delta\tau_r \quad (2)$$

$$\dot{\theta}_c^+ = \dot{\theta}_c c/U = 0.5\dot{\theta}_1^+\{1 - \cos[2\pi(\tau - \tau_{\rm cl})/\Delta\tau_{\rm cl}]\}$$
$$\tau_{\rm cl} \le \tau \le \tau_{\rm cl} + \Delta\tau_{\rm cl} \quad (3)$$

where $\dot{\theta}_0^+$, $\dot{\alpha}_0^+$, and $\dot{\theta}_1^+$ are constants, U is the reference velocity (defined later), and τ is the nondimensional time, $\tau = tU/c$, where t is the time. Here, τ_0 is the time at which the stroke cycle starts and $\Delta\tau_f$ is the fling duration; τ_r is the time at which the flip rotation starts and $\Delta\tau_r$ is the flip duration; and $\tau_{\rm cl}$ is the time at which the clap starts and $\Delta\tau_{\rm cl}$ is the clap duration. In the present study, rotation around the vertical axis is termed translation. The angular velocity of wing translation is given as

$$\dot{\phi}^+ = \dot{\phi} c/U = 0.5\dot{\phi}_0^+\{1 - \cos[2\pi(\tau - \tau_0)/\Delta\tau_s]\}$$
$$\tau_0 \le \tau \le \tau_0 + \Delta\tau_s \quad (4)$$

$$\dot{\phi}^+ = \dot{\phi} c/U = -0.5\dot{\phi}_0^+\{1 - \cos[2\pi(\tau - \tau_0 - \Delta\tau_s)/\Delta\tau_s]\}$$
$$\tau_0 + \Delta\tau_s \le \tau \le \tau_0 + 2\Delta\tau_s \quad (5)$$

where $\dot{\phi}_0^+$ is a constant, $\Delta\tau_s$ is the duration of the down- or upstroke. The velocity of upward motion near the end of the cycle, W, is given as

$$W^+ = W/U = 0.5W_0^+\{1 - \cos[2\pi(\tau - \tau_{\rm cl} - \Delta\tau_{\rm cl})/\Delta\tau_{\rm up}]\}$$
$$\tau_{\rm cl} + \Delta\tau_{\rm cl} \le \tau \le \tau_0 + \tau_c \quad (6)$$

where W_0^+ is a constant, $\Delta\tau_{\rm up}$ is the duration of the upward motion, and τ_c is the nondimensional stroke period. During the translation of the down- or upstroke, the angle of attack of the wing is constant and is denoted α_m. In most calculations α_m is specified as 40-deg. Parameters τ_c, $\Delta\tau_f$, $\Delta\tau_r$, $\Delta\tau_{\rm cl}$, $\Delta\tau_s$, $\Delta\tau_{\rm up}$, and α_m will be determined using flight data. Other parameters and constants in Eqs. (1–6) are related to these parameters.

B. Navier–Stokes Equations and Solution Process

The Navier–Stokes equations are numerically solved using moving overset grids. For flow past a body in arbitrary motion, the governing equations can be cast in an inertial frame of reference using a general time-dependent coordinate transformation to account for the motion of the body. The nondimensionalized incompressible unsteady Navier–Stokes equations, written in the inertial coordinate system *oxyz* (Fig. 2), are as follows:

$$\frac{\partial u}{\partial x} + \frac{\partial v}{\partial y} + \frac{\partial w}{\partial z} = 0 \quad (7)$$

$$\frac{\partial u}{\partial \tau} + u\frac{\partial u}{\partial x} + v\frac{\partial u}{\partial y} + w\frac{\partial u}{\partial z} = -\frac{\partial p}{\partial x} + \frac{1}{Re}\left(\frac{\partial^2 u}{\partial x^2} + \frac{\partial^2 u}{\partial y^2} + \frac{\partial^2 u}{\partial y^2}\right) \quad (8)$$

$$\frac{\partial v}{\partial \tau} + u\frac{\partial v}{\partial x} + v\frac{\partial v}{\partial y} + w\frac{\partial v}{\partial z} = -\frac{\partial p}{\partial y} + \frac{1}{Re}\left(\frac{\partial^2 v}{\partial x^2} + \frac{\partial^2 v}{\partial y^2} + \frac{\partial^2 v}{\partial y^2}\right) \quad (9)$$

$$\frac{\partial w}{\partial \tau} + u\frac{\partial w}{\partial x} + v\frac{\partial w}{\partial y} + w\frac{\partial w}{\partial z} = -\frac{\partial p}{\partial z} + \frac{1}{Re}\left(\frac{\partial^2 w}{\partial x^2} + \frac{\partial^2 w}{\partial y^2} + \frac{\partial^2 w}{\partial y^2}\right) \quad (10)$$

where u, v, and w are three components of the nondimensional velocity and p is the nondimensional pressure. In the nondimensionalization, U, c, and c/U are taken as the reference velocity, length, and time, respectively; $Re = Uc/\nu$, where ν is the flow viscosity coefficient. Equations (7–10) are solved using an algorithm based on the method of artificial compressibility. The algorithm was first developed by Rogers and Kwak[17] and Rogers et al.[18] for single-zone grid, and it was extended by Rogers[19] and Rogers and Pulliam[20] to overset grids. It is outlined next.

The equations are first transformed from the Cartesian coordinate system x, y, z, τ to the curvilinear coordinate system ξ, η, ζ, τ using a general time-dependent coordinate transformation. For a flapping wing in the present study, a body-fixed coordinate system, $o'x'y'z'$, is also employed (Fig. 2). The inertial coordinates o, x, y, z are related to the body-fixed coordinates $o'x'y'z'$ through a known relationship, and the transformation metrics in the inertial coordinate system $(\xi_x, \xi_y, \xi_z, \xi_\tau)$, $(\eta_x, \eta_y, \eta_z, \eta_\tau)$, and $(\zeta_x, \zeta_y, \zeta_z, \zeta_\tau)$, which are needed in the transformed Navier–Stokes equations, can be calculated from those in the body-fixed, noninertial coordinate system $(\xi_{x'}, \xi_{y'}, \xi_{z'})$, $(\eta_{x'}, \eta_{y'}, \eta_{z'})$, and $(\zeta_{x'}, \zeta_{y'}, \zeta_{z'})$, which need to be calculated only once.

The time derivatives of the momentum equations are differenced using a second-order, three-point backward-difference formula. To solve the time-discretized momentum equations for a divergence free velocity at a new time level, a pseudotime level is introduced into the equations and a pseudotime derivative of pressure divided by an artificial compressibility constant is introduced into the continuity equation. The resulting system of equations are iterated in pseudotime until the pseudotime derivative of pressure approaches zero, and thus, the divergence of the velocity at the new time level approaches zero. The derivatives of the viscous fluxes in the momentum equation are approximated using second-order central differences. For the derivatives of convective fluxes, upwind differencing based on the flux-difference splitting technique is used. A third-order upwind differencing is used at the interior points, and a second-order upwind differencing is used at points next to boundaries. Details of this algorithm may be found in Refs. 17 and 18.

With overset grids, as shown in Fig. 3, for each wing there is a body-fitted curvilinear grid, which extends a relatively short distance from the body surface, and in addition, there is a background Cartesian grid, which extends to the far-field boundary of

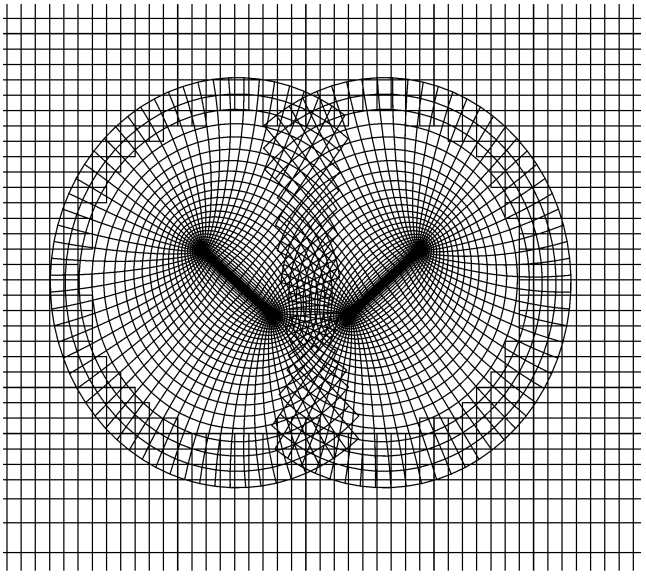

Fig. 3 Portions of moving overset grids.

the domain. The solution method for single grid is applied to each of the three grids. The wing grids capture features such as boundary layers, separated vortices, and vortex/wing interactions. The background grid carries the solution to the far field. The two wing grids are overset onto the background Cartesian grid, and parts of the two wing grids overlap when the two wings move close to each other. As a result of the oversetting of the grids, there are hole regions in the wing grids and in the background grid. As the wing grids move, the holes and hole boundaries change with time. To determine the hole-fringe points, the method known as domain connectivity functions by Meakin[21] is employed. Intergrid boundary points are grid points at the outer boundaries of the wing grids and the hole-fringe points. Data are interpolated from one grid to another at the hole-fringe points and, similarly, at grid points at the outer-boundary points of the wing grids. In the present study, the background grid does not move, and the two wing grids move in the background grid. The wing grids are generated using a Poisson solver that is based on the work of Hilgenstock.[22] They are O–H-type grids. The background Cartesian grid is generated algebraically. For computations in the present study, the artificial compressibility constant is set to 200. (It has been shown that when the artificial compressibility constant varied between 50 and 500, the number of subiteration changes a little, but the final result does not change.)

For far-field boundary conditions, at the inflow boundary, the velocity components are specified as freestream conditions, whereas pressure is extrapolated from the interior. At the outflow boundary, pressure is set equal to the freestream static pressure, and the velocity is extrapolated from the interior. On the wing surfaces, impermeable wall and no-slip boundary conditions are applied, and the pressure on the boundary is obtained through the normal component of the momentum equation written in the moving coordinate system.

Once the Navier–Stokes equations are numerically solved, the fluid velocity components and pressure at discretized grid points for each time step are available. The aerodynamic force acting on the wing is contributed by the pressure and the viscous stress on the wing surface. Integrating the pressure and the viscous stress over the wing surface at a time step gives the total aerodynamic force acting on the wing at the corresponding time instant. The lift of the wing L is the z component of the total aerodynamic force, and the drag of the wing D is the component of the total aerodynamic force parallel to the translational velocity of the wing. The force coefficients, denoted by C_L and C_D, respectively, are defined as follows: $C_L = L/0.5\rho U^2 S$ and $C_D = D/0.5\rho U^2 S$, where ρ is the fluid density and S is the wing area.

C. Data of Hovering Flight in *Encarsia formosa*

The only nondimensional parameter in the Navier–Stokes equations that needs to be specified is Re Reynolds number. For the flapping motion described by Eqs. (1–6), as already mentioned, nondimensional parameters τ_c, $\Delta\tau_f$, $\Delta\tau_r$, $\Delta\tau_{\rm cl}$, $\Delta\tau_s$, $\Delta\tau_{\rm up}$, and α_m need to be specified. They are computed based on the data of a hovering *Encarsia formosa*.[4,15] The data are as follows: Insect weight is 2.45×10^{-2} dyne, stroke amplitude Φ is approximately 135 deg, and stroke frequency n is 400 Hz. Wing length R is 0.65 mm, wing area (two wings) is 0.34 mm^2, and the mean chord length c is 0.26 mm.

The reference velocity is defined as $U = 2\Phi n r_2$, where r_2 is the radius of the second moment of wing area, $r_2 = 0.69\,R$, and is computed as 84.8 cm $\cdot$ s^{-1}. The Reynolds number and nondimensional period are computed as follows: $Re = cU/\nu = 15.3$, where $\nu = 0.144$ cm$^2 \cdot$ s^{-1}, and $\tau_c = (1/n)/(c/U) = 8.15$. From his study, Weis-Fogh[4] obtained the approximate time durations of the fling, flip, clap, etc. On the basis of these data (Fig. 6 of Ref. 4), we set $\Delta\tau_f = 0.11\tau_c$, $\Delta\tau_r = 0.17\tau_c$, $\Delta\tau_{\rm cl} = 0.11\tau_c$, $\Delta\tau_{\rm up} = 0.06\tau_c$, and $\Delta\tau_s = 0.47\tau_c$.

III. Results and Discussion

A. Test of Flow Solver

A single-grid solver based on the computational method[17,18] described earlier was developed by Lan and Sun.[23] It was tested by the measured unsteady forces on a flapping model fruit fly wing[24] and on a revolving model bumblebee wing.[25] A moving overset-grid solver was developed by the same authors, and it was tested by comparison with the analytical solution of the starting flow around a sphere and with the measured forces on a flapping model fruit fly wing.[26] The three-dimensional moving overset-grid solver is further tested here in two ways.

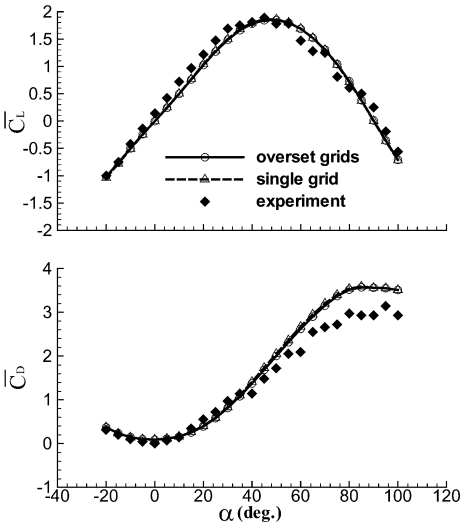

Fig. 4 Calculated and measured[26] lift and drag of revolving model wing including single-grid code[24] results.

First the code is tested using the recent experimental data of Usherwood and Ellington[27] of a revolving model bumblebee wing. In the computation, the wing rotated 120 deg after the initial start, and Re was set as 1800. (This Reynolds number Re value was similar to that of the bumblebee wing.) To make comparisons with the experimental data, lift and drag coefficients were averaged between 60 and 120 deg from the end of the initial start of rotation. (The averaged lift and drag coefficients are denoted by $\bar{C}_L$ and $\bar{C}_D$, respectively.) The computed and measured $\bar{C}_L$ and $\bar{C}_D$ are shown in Fig. 4. Results computed by the single-grid code[25] are included for comparison. In the computation, the wing grid has the dimensions $109 \times 50 \times 52$ around the wing section, in the normal direction and in the spanwise direction, respectively; the outer boundary of the wing grid is approximately $2.0c$ from the wing. The background Cartesian grid has dimensions $90 \times 85 \times 80$, and the outer boundary is $20c$ from the wing. The nondimensional time step is 0.02. In the entire α range (from -20 to 100 deg), the computed $\bar{C}_L$ agrees well with the measured values; both have approximately sinusoidal dependence on α. The computed $\bar{C}_D$ also agrees well with the measured values except when α is larger than $\sim$60 deg. The results computed by the overset grids are almost identical to those by the single-grid code.

Next, the code is tested by comparing with the force measurements[11] of an airfoil pair in fling motion. The angular velocity of the airfoils and the Reynolds number were taken as the same as that given in the experiment. At the beginning of the simulation, two wings were held parallel to each other at angle of attack $\alpha = 90$ deg, and the distance between the wings was set to $0.06c$. The wings were then rotated apart along their trailing edge. The exact wing motions used in their simulation and the experiment of Spedding and Maxworthy[11] are shown in Fig. 5a. The lift forces as functions of time for the calculation and the experiment are shown in Fig. 5b. In the computation, the wing grid has dimensions 153×55 around the wing section and in the normal direction respectively; the outer boundary of the wing grid is $2.5c$ from the wing. The background grid has dimensions 119×199 in the x and z directions, respectively. There is reasonably good agreement between the computation and the experiment.

B. Time Courses of Forces and Flows

As seen in Fig. 2, d is the distance between the two wings at the start of a stroke cycle. When d is very small, the motion between

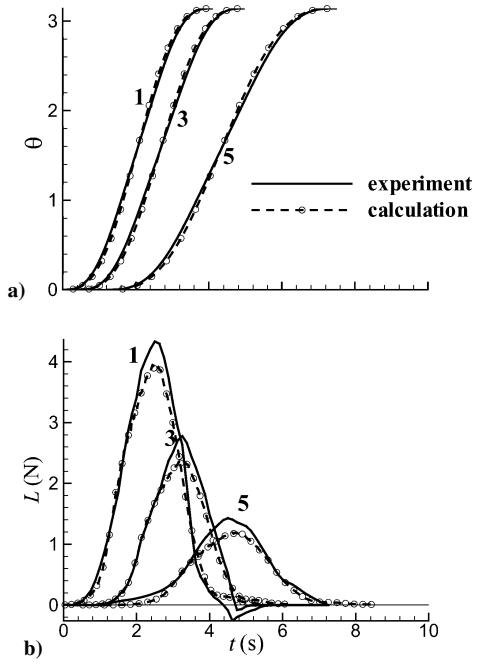

Fig. 5 Comparison between experimentally measured[9] and computed lift L during fling, where θ is opening angle.

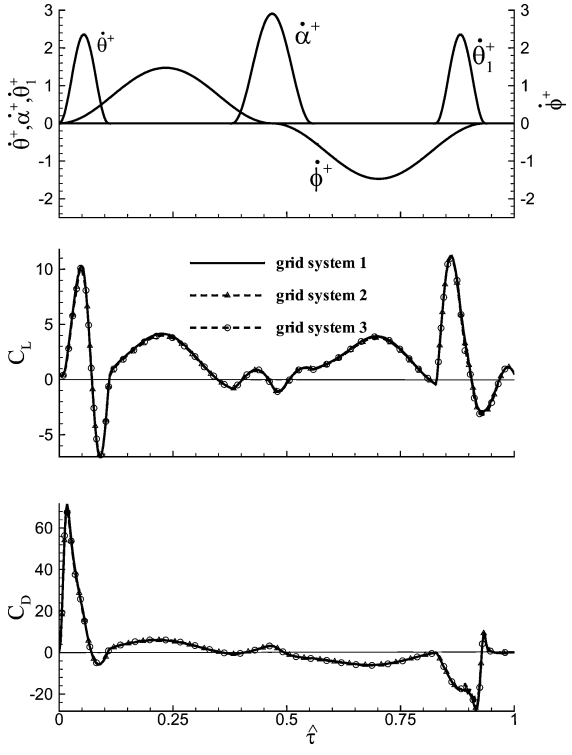

Fig. 6 Lift and drag coefficients vs nondimensional time in one cycle ($d = 0.1c$).

$\tau = \tau_0$ and $\tau = \tau_0 + \Delta\tau_f$ is a close approximation to the fling motion of the *Encarsia formosa*. Here, we specify $d = 0.1c$. (The effects of varying d will be investigated later.) Figure 6 shows the time courses of the motion and the aerodynamic force coefficients of the right wing in one cycle. Figure 7 shows the contours of the nondimensional spanwise component of vorticity at midspan location at the end of the fling. In Fig. 7, the magnitude of the nondimensional vorticity at the outer contour is 1 and the contour interval is 1. To correlate force and flow information, we express time during a

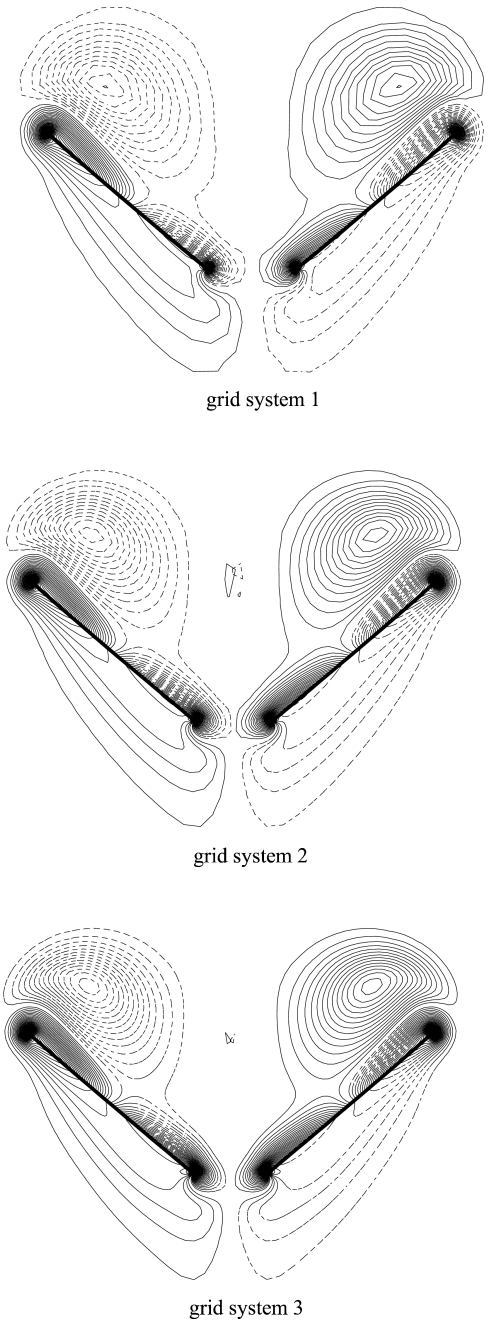

Fig. 7 Contours of nondimensional spanwise component of vorticity at midspan location at end of fling: ——, positive vorticity and - - - -, negative vorticity.

stroke cycle as a nondimensional parameter $\hat{\tau}$, such that $\hat{\tau} = 0$ at the start of the downstroke and $\hat{\tau} = 1$ at the end of the subsequent upstroke. Results calculated with three grid systems are plotted. In all of the grid systems, the outer boundary of the wing grid is set at about $2.5c$ from the wing surface and that of the background grid at $25c$ from the wings. For grid-system 1, the wing grid has dimensions $23 \times 49 \times 36$ in the normal direction, around the wing, and in the spanwise direction, respectively, and the background grid has dimensions $63 \times 53 \times 63$ in the x, y, and z directions, respectively. For grid-system 2, the corresponding grid dimensions are $32 \times 77 \times 50$ and $83 \times 63 \times 83$. For grid-system 3, the corresponding grid dimensions are $55 \times 105 \times 73$ and $113 \times 83 \times 113$. For all three grid systems, grid points of the background grid concentrate in the near field of the wings where its grid density is approximately the same as that of the outer part of the wing grid. It is observed that the first grid refinement produces some change in the vorticity

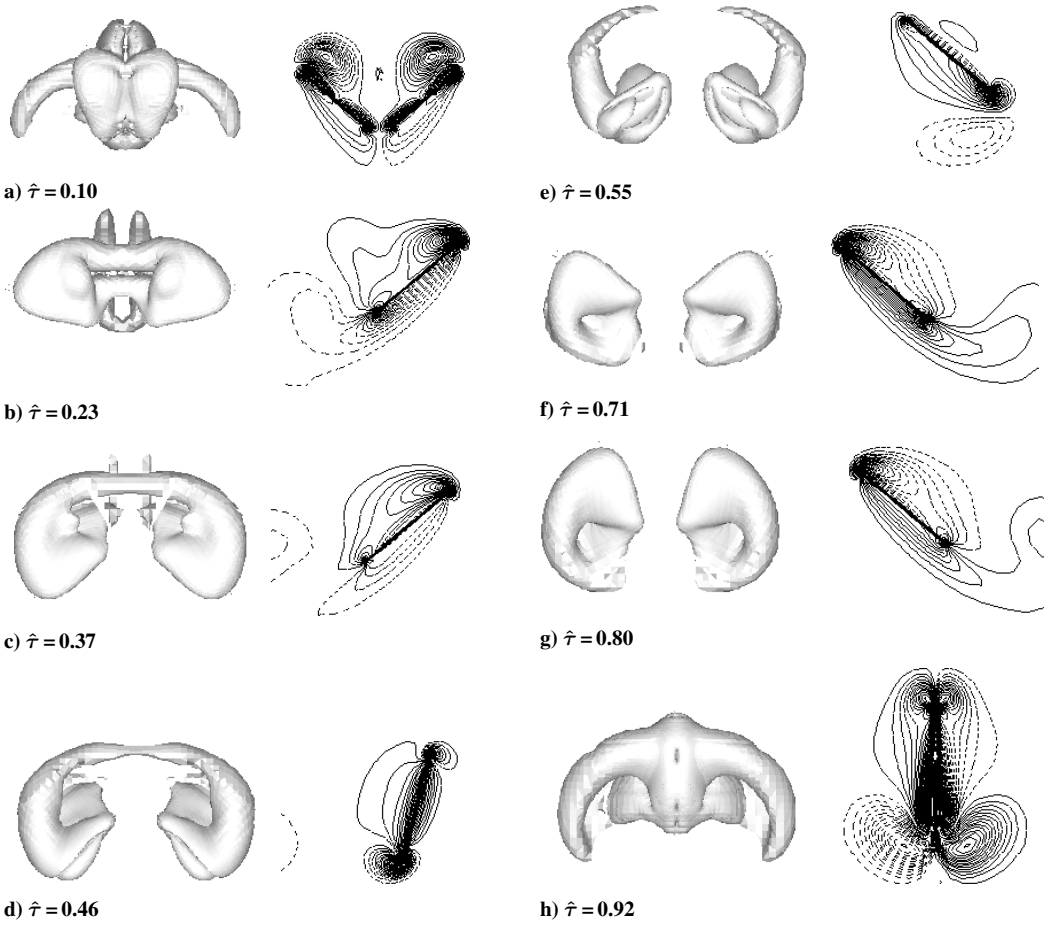

Fig. 8 Isovorticity surface plots (left) and sectional vorticity contour plots (right) at various nondimensional times ($d = 0.1c$): ——-, positive vorticity and - - - -, negative vorticity.

plot (Fig. 7); however, after the second grid refinement, the discrepancies are considerably reduced. There is almost no difference between the force coefficients calculated by the three grid systems (Fig. 6). Calculations were also conducted using a larger computational domain. The domain was enlarged by adding more grid points to the outside of the background grid of grid-system 2. The calculated results showed that there was no need to put the outer boundary farther than that of grid-system 2. From the preceding discussion, it is concluded that grid-system 2 is proper for the present study. (The effect of time step value was considered, and it was found that a numerical solution effectively independent of the time step was achieved if $\Delta\tau \leq 0.02$; therefore, $\Delta\tau = 0.02$ is used in the present study.)

Now, we proceed to analyze the time course of the force coefficients shown in Fig. 6 using the flowfield information. Figure 8 shows the isovorticity-surface plot (top view) and the contour plot of the spanwise component of vorticity at the midspan location at various times of the cycle. For the isosurface plot, the magnitude of the nondimensional vorticity is 1. For the sectional vorticity plot, the magnitude of the nondimensional vorticity at the outer contour is 1 and the contour interval is 1. Because the forces and flows of the left and right wings are similar, we only discuss those of the right wing. First, we examine the fling phase (Fig. 6; $\hat{\tau} = 0 - 0.11$): C_L increases to a peak value of approximately 10 at the middle of the fling phase and drops to negative value near the end of this phase, and C_D behaves similarly. A positive strong LEV is produced near the right wing, and a negative LEV of the same strength is produced near the left wing (Fig. 8a). That is, a strong LEV pair or vortex ring (when the two LEVs connect by the tip vortices form a vortex ring) is produced in a short period, and the time rate of change of the fluid impulse must be large. This explains the large peaks in C_L and C_D in this phase. The dip in C_L and C_D near the end of this phase is caused by the angular deceleration of the wing. When the angular velocity of the fling is decreasing, the wings are pushed by the flow on its upper surface, resulting in the decrease in the force coefficients.

Next, we examine the clap phase (Fig. 6; $\hat{\tau} = 0.83 - 0.94$). Near the end of the upstroke, the wing pair claps. Peaks in C_L and C_D as large as those during the fling are produced. Again, the large force peaks can be explained by the generation of a strong vortex pair or vortex ring in a short period (Fig. 8h). At the end of the cycle ($\hat{\tau} \approx 0.9 - 1.0$), there is a negative peak in C_L. This is caused partially by the angular deceleration of the wing in the later part of the clap and partially by the upward motion of the wing pair. The wing pair moves upward by a distance of $0.36c$ between $\hat{\tau} = 0.9$ and 1.0.

Figure 9 shows the velocity vectors in a vertical plane at the middle of the wing length. This can provide a physical explanation to the large lift during the fling or the clap: The fling (Figs. 9a and 9b) or the clap (Figs. 9c and 9d) produces a jet containing downward momentum, resulting in the large lift.

Finally, we consider the forces and flows between $\hat{\tau} = 0.11$ and 0.83, when the wing performs the translation of the downstroke ($\hat{\tau} \approx 0.11 - 0.38$), the flip ($\hat{\tau} = 0.38 - 0.55$), and the translation of the upstroke ($\hat{\tau} \approx 0.55 - 0.83$). Wing motion in this period is the same as that in normal flapping motion. (When the clap and fling is replaced by a flip similar to that at the end of the downstroke, the flapping motion is called normal flapping motion.) The flow of the wing pair performing normal flapping motion has been computed and the results will be presented here subsequently. It can be shown that C_L and C_D in this period are almost the same for the two types of flapping. That is, the clap and fling has little influence on the flows in the rest part of the stroke cycle. This might be because the LEV generated during the clap and fling is diffused rapidly and could not affect the flow in the subsequent phases. The rapid diffusion of the LEV generated during the clap

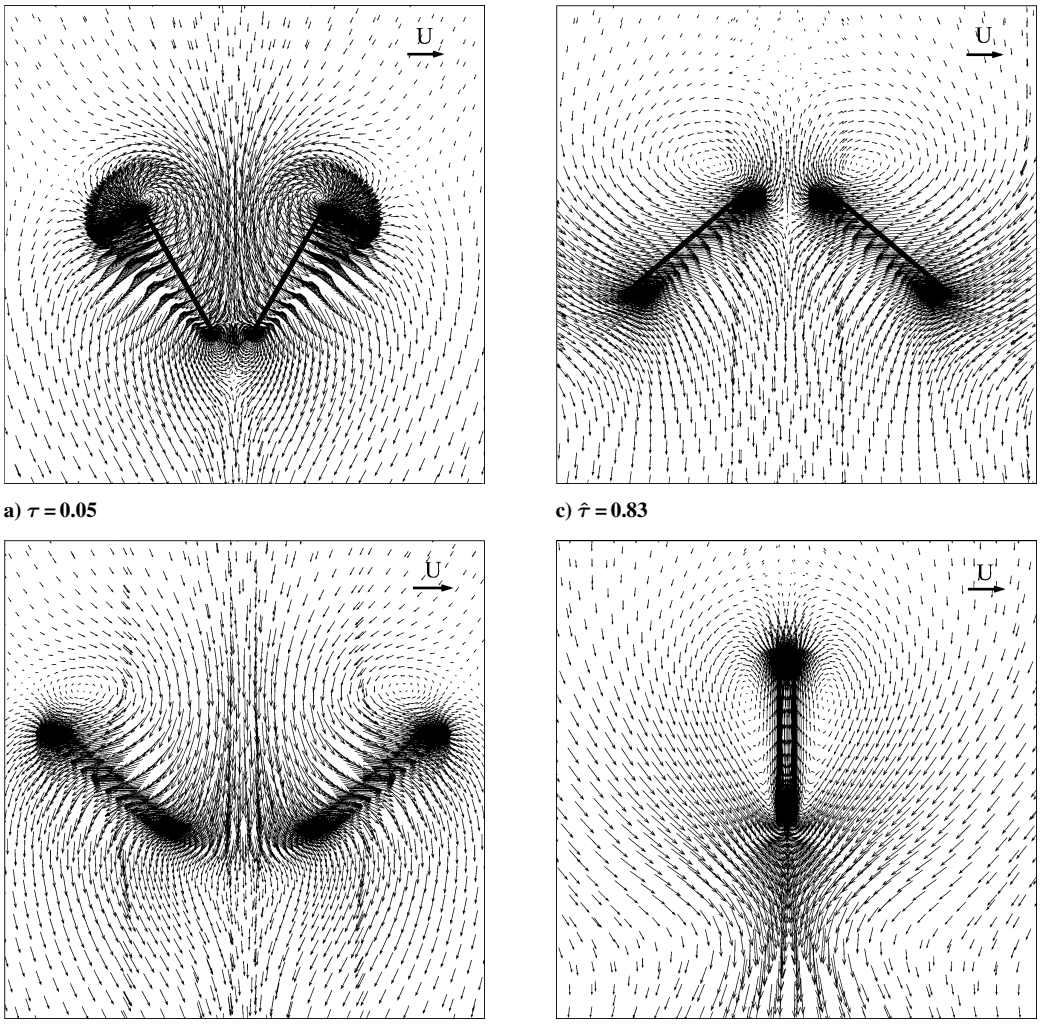

a) $\tau = 0.05$ c) $\hat{\tau} = 0.83$

b) $\hat{\tau} = 0.11$ d) $\hat{\tau} = 0.93$

Fig. 9 Velocity vectors in vertical plane at middle of wing length: horizontal arrow indicates reference velocity.

and fling can be seen clearly in Fig. 10, which shows the evolution of the LEV from the end of the clap and fling to a short time afterward. It is seen that at $\hat{\tau} = 0.105$ (the end of the clap and fling), the maximum nondimensional vorticity in the LEV is 12 (Fig. 10a), whereas at $\hat{\tau} = 0.193$ (9% of the flapping period afterward), this value becomes 3. This shows that the vorticity diffusion time scale is smaller than the time scale of flapping by about one order of magnitude.

In the downstroke translation ($\hat{\tau} = 0.23 - 0.46$) and the upstroke translation ($\hat{\tau} = 0.55 - 0.80$), a LEV (or thick vorticity layer) exists over the wing. It is of interest to examine, in the present case of very low Reynolds number Re ($Re = 15.3$), whether or not there is spanwise flow that could remove excess vorticity generated by separation at the leading edge. Figure 11 shows the velocity vectors in three planes normal to the upper surface of the wing at two time instants of the downstroke translation. Similar results exist for the upstroke translation. It is seen that spanwise flow directed from wing root to wing tip exists and the velocity of the spanwise flow is 10–50% of the reference velocity (the mean flapping velocity of the wing).

C. Mean Lift and Comparison with Insect Weight

Averaging C_L over one cycle gives the mean lift coefficient $\bar{C}_L$. The value of $\bar{C}_L$ for the described flapping motion with clap and fling is 1.78. The insect weight G, area of wing pair $2S$, and reference velocity U have already been given: $G = 2.45 \times 10^{-2}$ dyne, $2S = 3.35 \times 10^{-3}$ cm^2, and $U = 84.8$ cm $\cdot$ s^{-1}. Multiplying the mean lift coefficient, $\bar{C}_L = 1.79$, by $0.5\rho U^2 2S$ ($\rho = 1.23 \times 10^{-3}$ g $\cdot$ cm^{-3}) gives the mean lift as 2.64×10^{-2} dyne, which is approximately equal to the insect weight. As will be seen, using flapping without clap and fling, $\bar{C}_L$ is only 1.33, which is not sufficient for weight support.

Table 1 Effects of d on mean force coefficients

d/c	0.1	0.2	0.4	0.8	1.6	Single wing
$\bar{C}_L$	1.79	1.66	1.55	1.49	1.49	1.49
$\bar{C}_D$	6.29	4.92	4.49	4.26	4.17	4.14

D. Effect of d

Earlier the distance between the two wings at the start of a flapping cycle, d, was specified as $0.1c$. Here we investigate the effects of d. Figure 12 gives the time course of C_L and C_D in one cycle for various d. The results for a single wing performing identical motion as that of a wing of the wing pair are included for comparison. The corresponding mean force coefficients are shown in Table 1. When d is increased, the interference effect between the two wings decreases. When d is larger than $0.8c$, the force coefficients vary only slightly and are not very different from those of the single wing, indicating that when d is larger than approximately $0.8c$ the interference effects between the two wings become negligible.

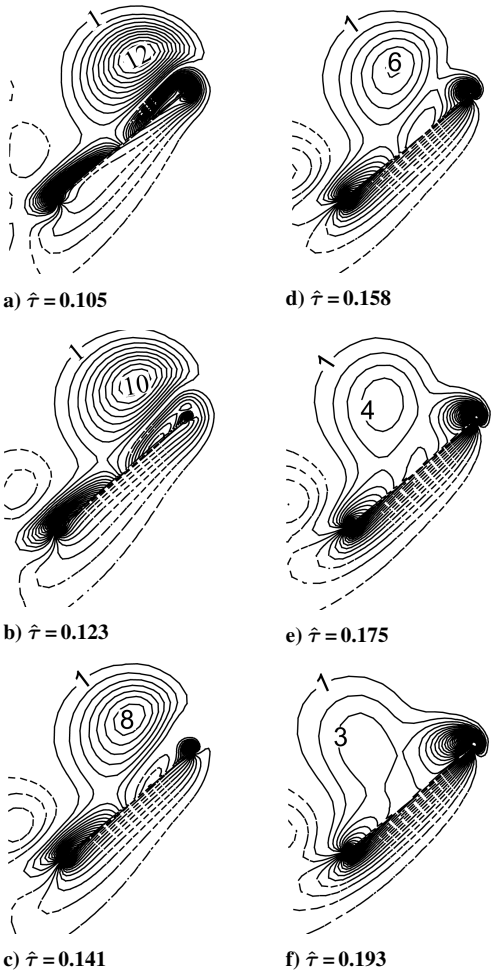

Fig. 10 Contours of nondimensional spanwise component of vorticity at midspan location, with rapid diffusion of LEV produced during clap and fling.

Comparing the results of the single wing with those of the case of $d = 0.1c$ shows that the peak in C_L during the fling (Fig. 12) is increased by 38% and $\bar{C}_L$ (Table 1) is increased by 20% by the interaction. Note (Fig. 12) that large interaction effects only occurs at the beginning of the fling phase ($\hat{\tau} \approx 0 - 0.05$) and at the end of the clap ($\hat{\tau} \approx 0.87 - 0.92$). In these periods, a large part of area of one wing is in close proximity to that of the other wing. This suggests that only when a large part of area of one wing is in close proximately to that of the other wing, the interaction effects could be large. Also note that when d increases from $0.1c$ to $0.2c$ the peak in C_L during the fling changes little, whereas the peak in C_D decreases by approximately 50%. This suggests that to have effective aerodynamic interaction, the wings should not be too close to each other.

E. Comparison with Normal Flapping Case

As already mentioned, when the clap and fling is replaced by a flip similar to that at the end of the downstroke, the flapping becomes normal flapping. C_L and C_D for normal flapping are shown in Fig. 13. Results for flapping with clap and fling are included for comparison. Between $\hat{\tau} = 0.11$ and 0.83 (the period after the clap and fling), C_L and C_D for the two types of flapping are almost identical. $\bar{C}_L$ and $\bar{C}_D$ for the case of normal flapping are 1.33 and 2.83, respectively, which are considerably smaller than those of the case of flapping with clap and fling ($\bar{C}_L = 1.79$ and $\bar{C}_D = 6.29$). Thus, we see that the fling produces a large lift peak at the beginning of a downstroke and the clap produces another one near the end of the subsequent upstroke, resulting in a value of $\bar{C}_L$ 34% larger than that of the corresponding normal flapping.

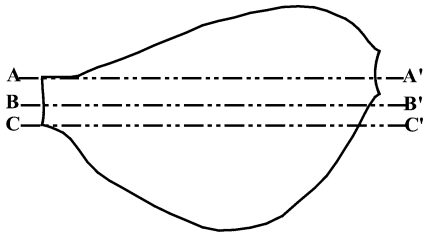

a) Locations of planes

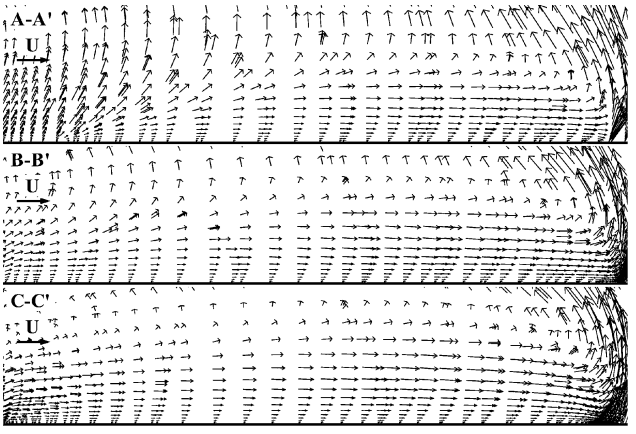

b) $\hat{\tau} = 0.23$

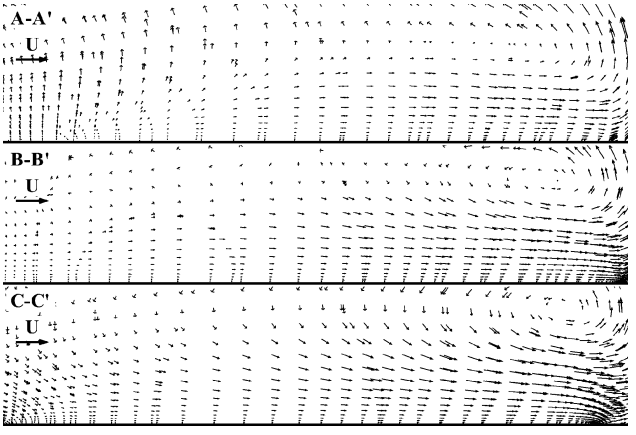

c) $\hat{\tau} = 0.37$

Fig. 11 Velocity vectors in planes normal to upper surface of wing.

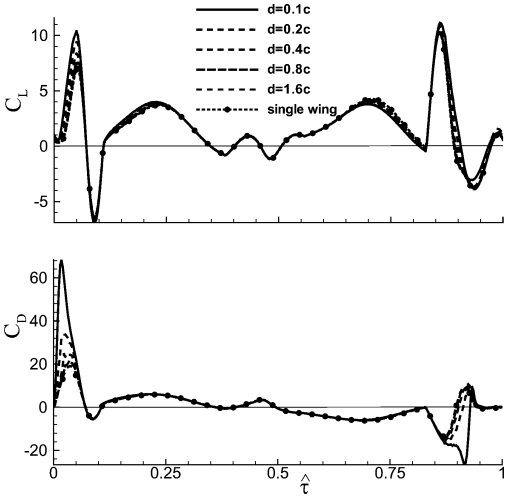

Fig. 12 Lift and drag coefficients vs nondimensional time in one cycle for various *d*.

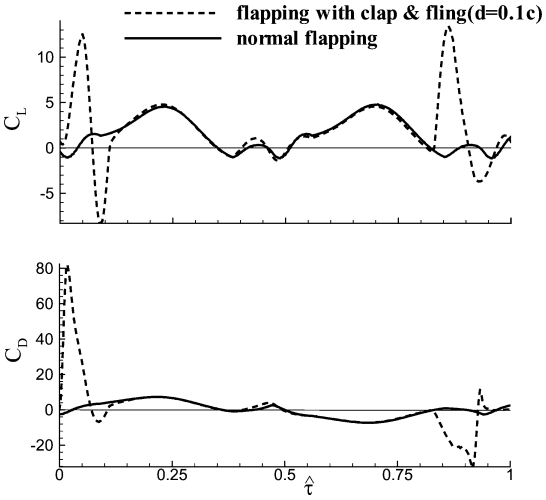

Fig. 13 Lift and drag coefficients vs nondimensional time in one cycle for flapping without and with clap and fling.

IV. Conclusions

The fling produces a large lift peak at the beginning of the downstroke, the mechanism of which is the generation of a vortex ring containing a downward jet in a short period; the clap produces a large lift peak near the end of the subsequent upstroke by a similar mechanism. Because the vorticity generated during the clap and fling diffuses rapidly, the clap and fling has little influence on the flows in the rest of the stroke cycle. The mean lift is sufficient to support the weight of the insect. The lift peaks due to the clap and fling result in more than a 30% increase in mean lift coefficient compared to the case of flapping without clap and fling.

References

[1]Ellington, C. P., "The Aerodynamics of Hovering Insect Flight. I. The Quasi-Steady Analysis," *Philosophical Transactions of the Royal Society B*, Vol. 305, Feb. 1984, pp. 1–15.

[2]Spedding, G. R., "The Aerodynamics of Flight," *Advances in Comparative and Environmental Physiology*, *Mechanics of Animal Locomotion*, Vol. 2, edited by R. M. Alexander, Springer-Verlag, London, 1992, pp. 51–111.

[3]Wang, J. Z., "Dissecting Insect Flight," *Annual Review of Fluid Mechanics*, Vol. 37, 2005, pp. 183–210.

[4]Weis-Fogh, T., "Quick Estimates of Flight Fitness in Hovering Animals, Including Novel Mechanism for Lift Production," *Journal of Experimental Biology*, Vol. 59, No. 1, 1973, pp. 169–230.

[5]Vogel, S., "Flight in Drosophila. II. Variations in Stroke Parameters and Wing Contour," *Journal of Experimental Biology*, Vol. 46, No. 2, 1967, pp. 383–392.

[6]Ellington, C. P., "The Aerodynamics of Hovering Insect Flight. III. Kinematics," *Philosophical Transactions of the Royal Society B*, Vol. 305, Feb. 1984, pp. 41–78.

[7]Lighthill, M. J., "On the Weis-Fogh Mechanism of Lift Generation," *Journal of Fluid Mechanics*, Vol. 60, 1973, pp. 1–17.

[8]Maxworthy, T., "Experiments on the Weis-Fogh Mechanism of Lift Generation by Insects in Hovering Flight. Part 1. Dynamics of the 'Fling,'" *Journal of Fluid Mechanics*, Vol. 93, 1979, pp. 47–63.

[9]Edwards, R. H., and Cheng, H. K., "The Separation Vortex in the Weis-Fogh Circulation-Generation Mechanism," *Journal of Fluid Mechanics*, Vol. 120, 1982, pp. 463–473.

[10]Wu, J. C., and Chen, H., "Unsteady Aerodynamics of Articulate Lifting Bodies," AIAA Paper 84-2184, Aug. 1984.

[11]Spedding, G. R., and Maxworthy, T., "The Generation of Circulation and Lift in a Rigid Two-Dimensional Fling," *Journal of Fluid Mechanics*, Vol. 165, 1986, pp. 247–272.

[12]Ro, K., and Tsutahara, M., "Numerical Analysis of Unsteady Flow in the Weis-Fogh Mechanism by the 3D Discrete Vortex Method with GRAPE3A," *Journal of Fluids Engineering*, Vol. 119, March 1997, pp. 96–102.

[13]Sun, M., and Yu, X., "Flows Around Two Airfoils Performing Fling and Subsequent Translation and Subsequent Clap," *Acta Mechanica Sinica*, Vol. 19, No. 2, 2003, pp. 103–117.

[14]Miller, L. A., and Peskin, C. S., "A Computational Fluid Dynamics of 'Clap and Fling' in the Smallest Insects," *Journal of Experimental Biology*, Vol. 208, No. 2, 2005, pp. 195–212.

[15]Ellington, C. P., "Non-Steady-State Aerodynamics of the Flight of *Encarsia formosa*," *Swimming and Flying in Nature*, Vol. 2, edited by T. Y. Wu, C. J. Brokaw, and C. Brenen, Plenum, New York, 1975, pp. 783–796.

[16]Sunada, S., Takashima, H., Hattori, T., Yasuda, K., and Kawachi, K., "Fluid-Dynamic Characteristics of a Bristled Wing," *Journal of Experimental Biology*, Vol. 205, No. 17, 2002, pp. 2737–2744.

[17]Rogers, S. E., and Kwak, D., "Upwind Differencing Scheme for the Time-Accurate Incompressible Navier–Stokes Equations," *AIAA Journal*, Vol. 28, No. 2, 1990, pp. 253–262.

[18]Rogers, S. E., Kwak, D., and Kiris, C., "Steady and Unsteady Solutions of the Incompressible Navier–Stokes Equations," *AIAA Journal*, Vol. 29, No. 4, 1991, pp. 603–610.

[19]Rogers, S. E., "On the Use of Implicit Line-Relaxation and Multi-Zonal Computations," AIAA Paper 91-1611, June 1991.

[20]Rogers, S. E., and Pulliam, T. H., "Accuracy Enhancements for Overset Grids Using a Defect Correction Approach," AIAA Paper 94-0523, Jan. 1994.

[21]Meakin, R. L., "On the Spatial and Temporal Accuracy of Overset Grid Methods for Moving Body Problems," AIAA Paper 94-1925, June 1994.

[22]Hilgenstock, A., "A Fast Method for the Elliptic Generation of Three Dimensional Grids with Full Boundary Control," *Num. Grid Generation in CFM'88*, edited by S. Sengupta, J. Hauser, P. R. Eiseman, and J. F. Thompson, Pineridge, Swansea, Wales, U.K., 1988, pp. 137–146.

[23]Lan, S. L., and Sun, M., "Aerodynamic Properties of a Wing Performing Unsteady Rotational Motions at Low Reynolds Number," *Acta Mechanica*, Vol. 149, March 2001, pp. 135–147.

[24]Sun, M., and Wu, J. H., "Aerodynamic Force Generation and Power Requirements in Forward Flight in a Fruit Fly with Modeled Wing Motion," *Journal of Experimental Biology*, Vol. 206, No. 17, 2003, pp. 3065–3083.

[25]Wu, J. H., and Sun, M., "Unsteady Aerodynamic Forces of a Flapping Wing," *Journal of Experimental Biology*, Vol. 207, No. 7, 2004, pp. 1137–1150.

[26]Sun, M., and Lan, S. L., "A Computational Study of the Aerodynamic Forces and Power Requirements of Dragonfly (*Aeschna junces*) Hovering," *Journal of Experimental Biology*, Vol. 207, No. 11, 2004, pp. 1887–1901.

[27]Usherwood, J. R., and Ellington, C. P., "The Aerodynamics of Revolving Wings. II. Propeller Force Coefficients from Mayfly to Quail," *Journal of Experimental Biology*, Vol. 205, No. 11, 2002, pp. 1565–1576.

C. Kaplan
Associate Editor